ORIGINAL ARTICLE

Journal of Cachexia, Sarcopenia and Muscle 2020; **11**: 1813–1829
Published online 13 September 2020 in Wiley Online Library (wileyonlinelibrary.com) **DOI:** 10.1002/jcsm.12618

Characterization of cachexia in the human fibrosarcoma HT-1080 mouse tumour model

Barbara Bernardo[1], Stephanie Joaquim[1], Jeonifer Garren[2], Magalie Boucher[3], Christopher Houle[3], Brianna LaCarubba[1], Shuxi Qiao[1], Zhidan Wu[1], Ryan M. Esquejo[1], Matthew Peloquin[1], Hanna Kim[1] & Danna M. Breen[1]*

[1]*Internal Medicine Research Unit, Pfizer Inc., Cambridge, MA, USA,* [2]*Biostatistics, Early Clinical Development, Pfizer Inc., Cambridge, MA, USA,* [3]*Drug Safety Research and Development, Pfizer Inc., Groton, CT, USA*

Abstract

Background Cancer cachexia is a complex metabolic disease with unmet medical need. Although many rodent models are available, none are identical to the human disease. Therefore, the development of new preclinical models that simulate some of the physiological, biochemical, and clinical characteristics of the human disease is valuable. The HT-1080 human fibrosarcoma tumour cell line was reported to induce cachexia in mice. Therefore, the purpose of this work was to determine how well the HT-1080 tumour model could recapitulate human cachexia and to examine its technical performance. Furthermore, the efficacy of ghrelin receptor activation via anamorelin treatment was evaluated, because it is one of few clinically validated mechanisms.

Methods Female severe combined immunodeficient mice were implanted subcutaneously or heterotopically (renal capsule) with HT-1080 tumour cells. The cachectic phenotype was evaluated during tumour development, including body weight, body composition, food intake, muscle function (force and fatigue), grip strength, and physical activity measurements. Heterotopic and subcutaneous tumour histology was also compared. Energy balance was evaluated at standard and thermoneutral housing temperatures in the subcutaneous model. The effect of anamorelin (ghrelin analogue) treatment was also examined.

Results The HT-1080 tumour model had excellent technical performance and was reproducible across multiple experimental conditions. Heterotopic and subcutaneous tumour cell implantation resulted in similar cachexia phenotypes independent of housing temperature. Tumour weight and histology was comparable between both routes of administration with minimal inflammation. Subcutaneous HT-1080 tumour-bearing mice presented with weight loss (decreased fat mass and skeletal muscle mass/fibre cross-sectional area), reduced food intake, impaired muscle function (reduced force and grip strength), and decreased spontaneous activity and voluntary wheel running. Key circulating inflammatory biomarkers were produced by the tumour, including growth differentiation factor 15, Activin A, interleukin 6, and TNF alpha. Anamorelin prevented but did not reverse anorexia and weight loss in the subcutaneous model.

Conclusions The subcutaneous HT-1080 tumour model displays many of the perturbations of energy balance and physical performance described in human cachexia, consistent with the production of key inflammatory factors. Anamorelin was most effective when administered early in disease progression. The HT-1080 tumour model is valuable for studying potential therapeutic targets for the treatment of cachexia.

Keywords Fibrosarcoma; HT-1080 tumour model; Cachexia; Food intake; Muscle force; Anamorelin

Received: 27 May 2020; Revised: 22 June 2020; Accepted: 7 July 2020
**Correspondence to: Danna M. Breen, Internal Medicine Research Unit, Pfizer Inc., 1 Portland Avenue, Cambridge, MA, USA. Email: danna.breen@pfizer.com*

Introduction

Cancer-associated cachexia is a debilitating multifactorial metabolic disease characterized by anorexia and body weight loss due to depletion of skeletal muscle mass and/or fat mass. Cachexia has a negative impact on quality of life, performance, chemotherapy treatment adherence, and overall survival of the patient.[1] Cancer cachexia is highly prevalent across many tumour types[2]; however, currently there are no effective therapies.

Although many rodent models have been developed, none are identical to the human disease. Therefore, the development of new preclinical models that simulate some of the physiological, biochemical, and clinical characteristics of the human disease is valuable. The most commonly used tumour models employ implanted tumour cell lines, such as colon 26 adenocarcinoma (C26) and Lewis lung carcinoma (LLC), with growing interest in the Kras, p53, Cre (KPC) pancreatic tumour model. These models have been reviewed extensively by others,[2–13] and several common limitations are noteworthy. Key technical limitations include numerous subclones that do not display cachexia or have a variable phenotype, and the cachexia phenotype varies according to tumour cell inoculation sites. The common biological limitations include rapid weight loss, which often correlates with aggressive and variable tumour growth and limits the number of days of treatment intervention; global gene expression changes in skeletal muscle that do not match cancer cachexia patient data; and a limited understanding of the clinical characteristics including anorexia, muscle function, and performance/activity. Beyond the tumour cell line models, genetically engineered tumour models have received much attention in recent years.[7,8,14,15] These models have high value but have limited accessibility, greater variability of disease onset, and progression, and tissue infiltration of the primary tumour and/or metastases can complicate interpretation of anti-cachexia treatments.

Many rodent tumour model studies have focused only on examining body weight and muscle mass.[8,16–18] Although these are important measurements for signs of efficacy, endpoints relating to physical activity and quality of life are critical for building translation to patients, especially, given the lack of success in demonstrating that increases in muscle mass also result in improved function. Rodent tumour models can be leveraged to compare a variety of endpoints related to physical function and activity including skeletal muscle function (force and fatigue independent of behaviour), grip strength, locomotion, and voluntary exercise.

The HT-1080 human fibrosarcoma cell line is commonly used as a rodent tumour model to study the effects of anti-cancer mechanisms.[19–21] Although sarcomas are not considered highly cachectic tumours, HT-1080 tumours secrete several relevant pro-cachectic factors such as growth differentiation factor 15 (GDF-15), interleukin 6 (IL-6), and Activin A, and it has been reported that this tumour model has a cachexia phenotype.[22] Thus, the HT-1080 tumour model could provide a valuable opportunity to understand anti-cachexia treatments. Therefore, the purpose of this paper was to determine whether the HT-1080 tumour model overcomes the technical and physiological limitations discussed and recapitulates the physiological, biochemical, and clinical characteristics of human cachexia. Furthermore, the efficacy of ghrelin receptor activation was evaluated for model validation because it is one of few mechanisms supported by clinical efficacy data.

Material and methods

Animals

Female severe combined immunodeficient ICR-Prkdc mice (8–12 weeks) were obtained from Taconic Farms Inc. (Rensselaer, NY, USA). All mice were maintained on a standard light–dark cycle (6 a.m.–6 p.m.) and were allowed *ad libitum* access to water and food (Purina rodent diet 5061; Purina Mills, St. Louis, MO, USA). All mice were housed individually at standard housing temperatures (22 ± 1°C) or at thermoneutral conditions (27 ± 1°C) as indicated. Prior to tumour implantation, mice were acclimated to experimental conditions for 2 weeks. All procedures were approved by the Pfizer Groton and Cambridge Animal Care and Use Committees (Animal Use Protocols GTN-01133 and KSQ-01127), in accordance with the ethical standard laid down in the 1964 Declaration of Helsinki and its later amendments.

HT-1080 cell culture

HT-1080 cells [HT-1080 (HT1080) (ATCC® CCL-121™)] were purchased from the American Type Culture Collection (Manassas, VA, USA) and stored in liquid nitrogen until use. Cells were maintained in Eagle's minimum essential medium supplemented with 10% (v/v) heat-inactivated foetal bovine serum, 1% minimum non-essential amino acids, 1% GlutaMAX, and 1% penicillin/streptomycin (Gibco) with incubators maintained at 37°C and 5% CO_2. Cells were sub-cultured in preparation for implant into animals. The cells were sub-cultured until the desired number of cells was reached to be used *in vivo*.

Generation of the HT-1080 tumour models

In the subcutaneous HT-1080 model, subcutaneous implantation was performed with a 200 μL injection of cell suspension [5 million cells suspended in equal parts of sterile Matrigel®

(Corning®, Tewksbury, MA, USA) and phosphate-buffered saline (PBS)] in the flank region without anaesthesia.

In the heterotopic HT-1080 model, renal subcapsular tumour cell implantation was performed via laparotomy under isoflurane anaesthesia using a stereo-microscope (Leica M651; Leica Microsystems AG, Heerbrugg, Switzerland). Mice received a pre-operative analgesic (Meloxicam SR™, 4 mg/kg, subcutaneous injection). During surgery, the caudal capsule of the left kidney was inoculated with 3 million HT-1080 cells suspended in equal parts of Matrigel® and PBS solution. Post-operative buprenorphine (0.1 mg/kg) was administered upon anaesthetic recovery and as needed on Days 1 and 2 post-operatively for pain relief. Mice were euthanized 15 days later by CO_2 asphyxiation. During necropsy, primary tumour volume was determined using a calliper, and abdominal visceral organs were inspected for macroscopically visible metastases. The primary tumour tissue was then harvested for histological evaluation.

Body weight, body composition, food intake, and tumour growth assessments

Body weight and food weight were measured daily following implantation using a digital scale (measured approximately between 8 and 10 a.m.). Food pellets (~8 g) were given each day in a ceramic bowl placed on the bottom of the cage. Food remaining from the previous day was measured and discarded. Body composition was measured prior to euthanasia via EchoMRI® (4-in-1, Houston, TX, USA). Tumour growth was monitored daily following inoculation and size was measured at minimum of three times per week using digital callipers (Mitutoyo, 500-171-30) when a palpable tumour was formed. Tumour weight was estimated using the following equation: Tumour weight = $(\text{width})^2 \times \text{length}/2$. Mice were euthanized when ≥30% body weight loss was achieved (minus tumour burden) and/or decline in overall health as defined by a predefined body condition scoring system was noted (*Table* S1).

Tissue collection and histology

At the end of the study, mice were euthanized by CO_2 inhalation, and plasma was collected via cardiac puncture. Tibialis anterior (TA), gastrocnemius–plantaris complex, soleus muscles from the hindlimb, and heart were carefully dissected out, weighed, and either immersed fixed in formalin and paraffin embedded or frozen in liquid nitrogen for further analysis. The subcutaneous and heterotopic tumours (including the kidney) were also collected, weighed, and immersion fixed in 10% neutral buffered formalin. Each tumour was sectioned longitudinally across its longest axis, placed into tissue cassettes, and embedded into paraffin blocks. In some instances, more than one block was needed to accommodate the larger tumours. One haematoxylin and eosin-stained slide was generated from each paraffin block and evaluated by a board-certified veterinary pathologist using light microscopy with a focus on identifying group differences in tumour cell morphology.

A subset of TA muscle was collected and frozen in OCT (Fisher Scientific, Pittsburgh, PA, USA). Samples were sectioned at 10 μm, placed on a Superfrost Plus Microscope Slide (Fisher Scientific, Pittsburgh, PA, USA), and post-fixed in 4% paraformaldehyde. Tissues were permeabilized in 0.1% Triton and incubated overnight in wheat germ agglutinin (WGA) Alexa Fluor 488 Conjugate (Invitrogen, Carlsbad, CA, USA) at 4°C. Following incubation, slides were rinsed in DBPS followed by distilled water. Slides were mounted in Prolong Diamond Antifade Reagent with 4′,6-diamidino-2-phenylindole (Invitrogen, Carlsbad, CA, USA). Slides were scanned on a Leica/VERSA whole slide fluorescent digital scanner (Leica Biosystems Inc. Buffalo Grove, IL, USA) using the ×20 magnification setting. Images were analysed using custom algorithms created with Visiopharm Image analysis software (Visiopharm, Westminster, CO, USA) and optimized for the target of interest. An initial application was created to identify and measure the muscle tissue as a region of interest (ROI). A second application was applied to each ROI, which used uniform thresholds to measure outlined WGA-stained cross-sectional area (CSA) of each muscle fibre. For each tissue section, raw data values were reported as the median fibre CSA, the fibre count, the total area of the muscle profile, and the tissue area.

Quantitative reverse transcriptase polymerase chain reaction

Ribonucleic acid was extracted and purified with RNeasy kits (Qiagen Inc., Germantown, MD, USA) and then reverse transcribed into complementary deoxyribonucleic acid (cDNA) with a High Capacity cDNA Reverse Transcription Kit (Applied Biosystems Inc., Foster City, CA, USA). Quantitative reverse transcriptase polymerase chain reaction (qRT-PCR) was performed using TaqMan reagents and primer-probes (Applied Biosystems Inc., Foster City, CA, USA). Catabolism genes in skeletal muscle [Atrogin-1 (*Fbxo32*); muscle ring finger 1, MuRF1 (*Trim63*); forkhead box O1, *Foxo1*] and autophagy (BCL2 interacting protein 3, *Bnip3*) were examined by qRT-PCR and normalized to the control gene, hypoxanthine phosphoribosyltransferase (*Hprt*).

Comprehensive laboratory animal monitoring system home cage

Whole-body energy metabolism was assessed utilizing a comprehensive laboratory animal monitoring system home

cage (CLAMS-HC) (Columbus Instruments, Columbus, OH, USA) following the manufacturer's instructions. On Day 7 post-cell implantation, non-tumour-bearing (NTB) mice and tumour-bearing mice were placed in a CLAMS. Data were collected every 15 min for each animal. Energy expenditure, resting energy expenditure, and oxygen consumption were calculated according to the manufacturer's instructions. Energy expenditure was evaluated both non-normalized and normalized to tumour-free body weight for each mouse. Ambulatory activity was measured utilizing the CLAMS-HC system configured with dual infrared photocell technology and was calculated utilizing an Opto-M4 Activity Monitor and a patented process for the tabulation of activity counts associated with ambulation.

Human and mouse plasma cytokine analysis

Cytokine levels were determined using the Mesoscale Discovery (MSD) Human Proinflammatory Panel 1 (K15049D) and Mouse Proinflammatory Panel 1 (K15048D) and performed using manufacturer instructions. Human or mouse Activin A (cannot distinguish between human and mouse) and GDF-15, were measured using human-specific or mouse-specific ELISA (R&D Systems, Minneapolis, MN, USA). Human/rodent GDF-8 and GDF-11 levels were determined using an immunoaffinity LC\MS workflow as previously described.[23]

Blood urine nitrogen and creatinine analysis

Blood was collected via cardiac puncture at the end of study and separated into serum. Serum blood urine nitrogen (BUN) and creatinine were determined by using Advia 1800 chemistry analyser (Siemens, Tarrytown, NY, USA) according to the manufacturer's manual. Creatinine was measured by formation of a complex of creatinine with alkaline picric acid at 505 nm. BUN was measured by the glutamate dehydrogenase and oxidation of NADH 340 nm at 37°C.

In vivo force and fatigue measurements

Mice were anaesthetized with isoflurane and placed supine on a platform heated via a circulating water bath at 37°C. The right leg was shaved up to the patella and right knee stabilized via knee clamp. Once stabilized, the right foot was affixed to a Dual Mode Foot Plate (300-C FP, Aurora Scientific Inc., Aurora, Canada), and two electrodes were placed subcutaneously near the mid-belly of the gastrocnemius to achieve plantar flexion. A 1 Hz electrical stimulation was delivered (0.2 s duration, 1 s between stimulations) via stimulator (701C, Aurora Scientific Inc.) while increasing amperes to generate a maximum twitch measurement. After a maximum twitch was established, a force frequency of isometric contractions was initiated (0.2 s duration, 120 s between stimulations). Mice were given 5 min of rest after the final contraction before initiating the fatigue protocol (50 contractions, 0.2 s duration, 2 s between stimulations). All data were collected and analysed using the manufacturer supplied software (DMC and DMA, Aurora Scientific Inc.). Mice were housed at thermoneutral temperature prior to analysis. Analysis was performed on Day 15 post-tumour implantation.

In situ force measurements

Mice were anaesthetized with isoflurane and placed supine on a platform heated via circulating water bath at 37°C. The skin was removed from the right leg exposing the TA muscle, and the lower ligament was tied with a looped suture at the head of the TA. The patella was secured to the heated platform with a 25-G needle, and the looped suture was fixed to the Dual Mode Muscle Lever (300-C, Aurora Scientific Inc.). Two electrodes were placed above the tibia and under the TA. A 1 Hz electrical stimulation was delivered (0.2 s duration, 1 s between stimulations) via stimulator (701C, Aurora Scientific Inc.), and tension of the TA was increased until an optimal tension was achieved (Lo). After optimal tension was established, a force frequency of isometric contractions was initiated (0.2 s duration, 120 s between stimulations). All data were collected and analysed using the manufacturer supplied software (DMC and DMA, Aurora Scientific Inc.). Mice were housed at thermoneutral temperature prior to this measurement.

Grip strength

Forearm grip strength was assessed on Day 16 post-tumour inoculation (thermoneutral housing conditions) by means of a grip strength meter (Columbus Instruments, Columbus, OH). The mouse grasped a mesh bar connected to a force transducer and was pulled gently by the tail until the grip was broken. The peak force (*g*) produced during the grip exercise was recorded by the transducer. The test was performed three times within 2 min for each animal, and the mean of the three attempts was recorded.

Voluntary locomotion measurements: Columbus wheel running and VIUM Digital Smart Cage

Voluntary running wheel distance was measured in mice housed in thermoneutral conditions with free access to

voluntary running wheels (Columbus Instruments, Chicago, IL, USA) and food and water *ad libitum* in a 12 h:12 h light: dark cycle room. Mice were acclimated in the cage with running wheels for 9 days, and they were then randomized according to their average body weights and motion over the last 3 days prior to HT-1080 implantation. Body weights and running distance were measured daily for 28 days. In a separate group of mice, average motion was measured using the VIUM Digital Smart Cages (VIUM Inc., San Mateo, CA, USA) with voluntary running wheel access. Mice were acclimated in the VIUM cages for 5 days, and they were randomized according to their average body weights and motion over the last 3 days prior to HT-1080 implantation. Body weights, and night-time and daytime motion were measured daily for 18 days.

Anamorelin prevention and intervention studies

Anamorelin (CAS 339539-92-3, BOC Sciences, New York, USA) was dissolved in deionized water at 3 mg/mL. The anamorelin dosing volume of 30 mg/kg was scaled according to the weight of each individual animal and administered once daily via oral gavage while vehicle groups received deionized water. The dose of anamorelin was chosen based on the weight gain efficacy reported in a lung cancer mouse xenograft model.[24] Animals were randomly assigned into each group (10 mice per group). Anamorelin treatment was initiated on Day 8 (prevention study) or Day 13 (intervention study) post-subcutaneous HT-1080 cell implantation. Mice were housed at thermoneutral temperature.

Statistical analysis

Mixed-effects models with appropriate correlation structure, terms, and variance adjustments are performed to test for associations between treatment groups over time. Multivariate analysis of variance or false discovery rate (FDR)-adjusted *t*-tests/Mann–Whitney tests are performed to test for multiple associations between treatment groups. Kolmogorov–Smirnov test was used to see if the data came from the similar distribution. Analysis of variance with appropriate terms and adjustments are performed to test for associations between more than two treatment groups. *t*-tests with appropriate terms and adjustments are performed to test for associations between two treatment groups. To identify any meaningful pairwise associations between treatment groups, pairwise contrasts are specified. All multiple comparisons use the FDR adjustment of the *P* values. All analyses are performed using R (Version 3.5).

Results

Heterotopic and subcutaneous tumour implantation result in similar cachexia and tumour phenotypes independent of housing temperature

Both the heterotopic (renal capsule) and subcutaneous implant models dramatically decreased body weight (>10%) ~10 days post-implantation (*Figure* 1A, E, S1A, B). Body weight continued to decline until the end of the study, reaching ~20–25% average weight loss. Both models resulted in fat (*Figure* 1B, F) and lean mass loss (*Figure* 1C, G). HT-1080 tumour-bearing mice, compared with NTB control mice, displayed a food 'grinding' behaviour where each night a substantial amount of food crumbs was observed on the cage bottom. Food grinding behaviour has been reported as part of an optimal food intake strategy where mice select the higher-energy-density components of the food.[25] We observed that this behaviour became more prominent with disease progression in the tumour-bearing mice, suggesting an adaptive survival response. This made it difficult to accurately assess food intake using standard hoppers. To limit food crumbs and spillage, a standard food allotment was given to the mice each day in a ceramic bowl. Food intake was decreased in tumour-bearing mice in both models (*Figure* 1D, H); however, a comparison across models is limited owing to the sensitivity challenges outlined in addition to the anorexic effect of surgery in the heterotopic model. To examine whether cold stress-induced basal metabolic changes impacted cachexia disease progression, the subcutaneous model was also evaluated at thermoneutral housing temperature (*Figure* 1I–L). Weight loss was modestly accelerated in the thermoneutral subcutaneous model compared with standard housing temperature, where 25% weight loss was achieved on Day 15 post-implantation at thermoneutrality vs. Day 19 at standard temperature (*Figures* 1E, I, S1B). Furthermore, body composition changes (fat and lean mass loss) were comparable at the end of the study, and both models had significantly reduced food intake (*Figure* 1E–L).

In the heterotopic model, tumour weight was assessed at the time of necropsy (Day 15). As the left kidney was excised along with the tumour (*Figure* S1C, 1.2 ± 0.2 g), terminal tumour weight was calculated by subtracting the weight of the right kidney (*Figure* 2A, 1.1 ± 0.2 g). Tumour growth in the subcutaneous model appeared to be slower than that of the heterotopic model. Subcutaneous tumour burden reached an average of ~0.5 g on Day 15 and then ~0.8 g at the end of the study on Day 21 (*Figure* 2C). The subcutaneous tumour model at thermoneutrality had slightly accelerated tumour growth as compared with standard housing temperature where tumour weight was ~0.9 g on Day 15 (*Figure* 2E). Only minimal tumour ulcerations or abrasions were observed

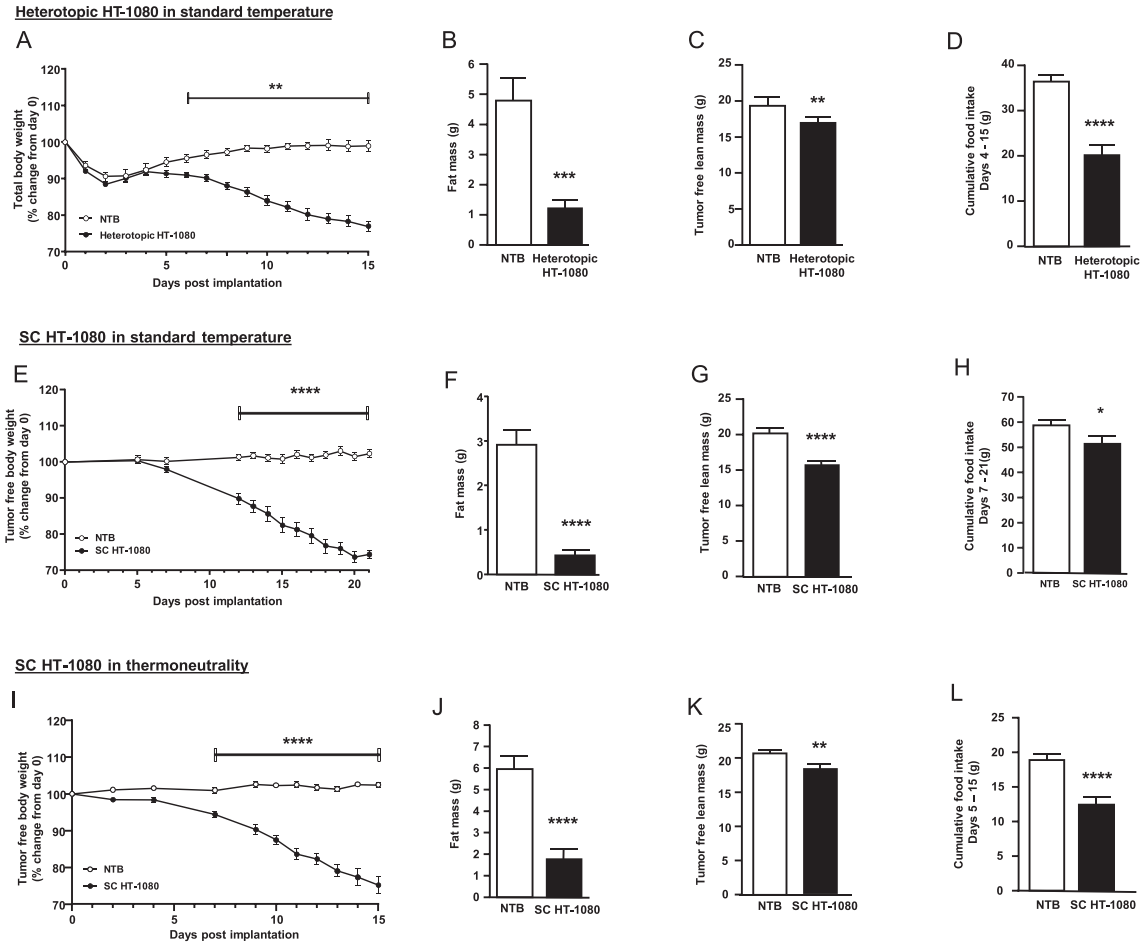

Figure 1 Heterotopic and subcutaneous HT-1080 tumour implantation result in similar changes in body weight, body composition, and food intake independent of housing temperature. *(A–D)* Heterotopic (renal capsule) HT-1080 tumour implantation at standard housing temperature decreased *(A)* body weight, *(B)* fat mass, *(C)* tumour-free lean mass, and *(D)* cumulative food intake (Days 4–15). n = 9–15 animals/group. *(E–H)* Subcutaneous HT-1080 tumour implantation at standard housing temperature decreased *(E)* tumour-free body weight, *(F)* fat mass, *(G)* tumour-free lean mass, and *(H)* cumulative food intake (Days 7–21). n = 9–10 animals/group. *(I–L)* Subcutaneous HT-1080 tumour implantation at thermoneutral housing temperature decreased *(I)* tumour-free body weight, *(J)* fat mass, *(K)* tumour-free lean mass, and *(L)* cumulative food intake (Days 5–15). n = 13–16 animals/group. $^{*}P < 0.05$; $^{**}P < 0.01$; $^{***}P < 0.001$; $^{****}P < 0.0001$; comparison of body weight changes with mixed-effects models; comparison of body composition and food intake with Student's t-test. Data represented as mean ± SEM. NTB = non-tumor bearing, SC = subcutaneous.

(~10% of mice). We also examined the microscopic appearance of the HT-1080 tumours in all three models in subsets of mice to determine if there were any morphological differences (*Figures* 2B, D, F and S1D). All tumours consisted predominantly of viable tumour tissue with variably sized areas of necrotic tissue often localized to central regions of the tumour (*Figure* 2B, D, and F; yellow asterisk indicates tumour cells; red asterisks indicates necrosis). There were no apparent group differences for any of these features, nor were there any group differences in the morphologic appearance of tumour cells (*Figures* 2B, D, F and S1D). A thin layer of fibrovascular stromal tissue was noted inconsistently around the periphery of most xenografts, with minimal amounts of inflammation occasionally observed as a secondary reaction to areas of necrosis. There was no indication of a primary inflammatory reaction directed towards viable tumour cells as was anticipated given the immunocompromised state of the host mice. Other studies have similarly described this tumour without reporting inflammation as a feature of this model.[26,27] The tumour cells exhibited morphological characteristics consistent with their fibroblastic origin, and there was a relatively high number of mitotic figures observed in each tumour with no apparent differences between treatment groups. In the heterotopic tumour model (renal capsule), serum BUN was not changed, and creatine levels were only modestly decreased in comparison with NTB mice (*Figure* S1E, F), indicating that kidney function was not impaired as a result of the heterotopic tumour. Because no profound differences were identified between models, all subsequent experimentation and data described were from the subcutaneous model under thermoneutrality (to eliminate any unknown confounding effects of cold stress) unless otherwise indicated.

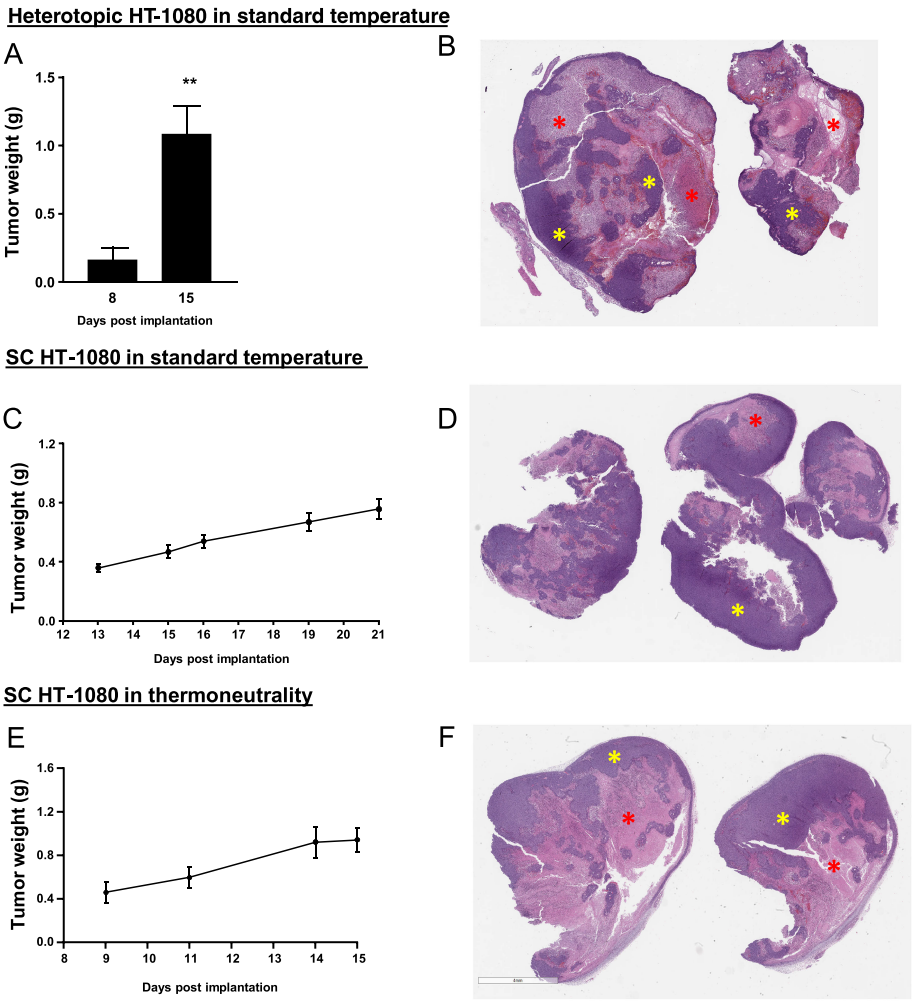

Figure 2 Heterotopic and subcutaneous HT-1080 tumour implantation result in comparable tumour growth and histological characteristics independent of housing temperature. *(A and B)* Heterotopic (renal capsule) HT-1080 tumour implantation at standard housing temperature; *(A)* approximate tumour weight on Day 8 (n = 3) and 15 (n = 13) post-implantation (right kidney weight subtracted from the weight of tumour with primary left kidney (*Figure* S1C) for each animal on Day 8 and Day 15) and *(B)* histology showing well-encapsulated tumour nodules with geographic necrosis. *(C and D)* Subcutaneous HT-1080 tumour implantation at standard housing temperature; tumour weight up to 21 days post-implantation (n = 10) and histology showing well-encapsulated tumour nodules with geographic necrosis. *(E and F)* Subcutaneous HT-1080 tumour implantation at thermoneutral housing temperature; tumour weight up to 15 days post-implantation (n = 16) and histology showing well-encapsulated tumour nodules with geographic necrosis. Sections were stained with haematoxylin and eosin. Scale bar (right panel): 4 mm. Yellow asterisks, tumour cells; red asterisks, necrosis. $^{**}P < 0.01$ by Student's t-test or mixed-effects models were applied for tumour weight as appropriate. Data are expressed as mean ± SEM. SC = subcutaneous.

Whole-body energy metabolism is reduced

To investigate the extent to which differences in whole-body energy metabolism may be involved in the progression of cachexia, we examined NTB and SC HT-1080 tumour-bearing animals by utilizing indirect calorimetry in a comprehensive laboratory animal monitoring system (CLAMS). NTB and SC HT-1080 tumour-bearing mice were evaluated starting at Day 8 post-implantation and through Day 18. Energy expenditure was reduced in tumour-bearing mice compared with NTB controls as early as Day 8 (*Figures* 3A, S2E), concurrent with the start of body weight decline (*Figure* S2A, B). This decrease in energy expenditure was sustained throughout tumour development and was more profound in the dark cycle with no differences demonstrated between animals during early-stage or late-stage cachexia despite the longer duration of anorexia at the later stage (*Figures* 3A, B, S2E). As tumour growth progressed (*Figure* S2C) and the cachectic phenotype worsened (*Figure* S2A, B, D), tumour-bearing mice demonstrated a reduction in respiratory exchange ratio (RER) compared with NTB mice during both diurnal and nocturnal periods, and this occurred as early as Day 8 (*Figure* 3A, B). Similarly, oxygen consumption (VO_2) in tumour-bearing mice was decreased as early as Day 8 and was sustained throughout tumour development (*Figure* 3A, B).

DOI: 10.1002/jcsm.12618

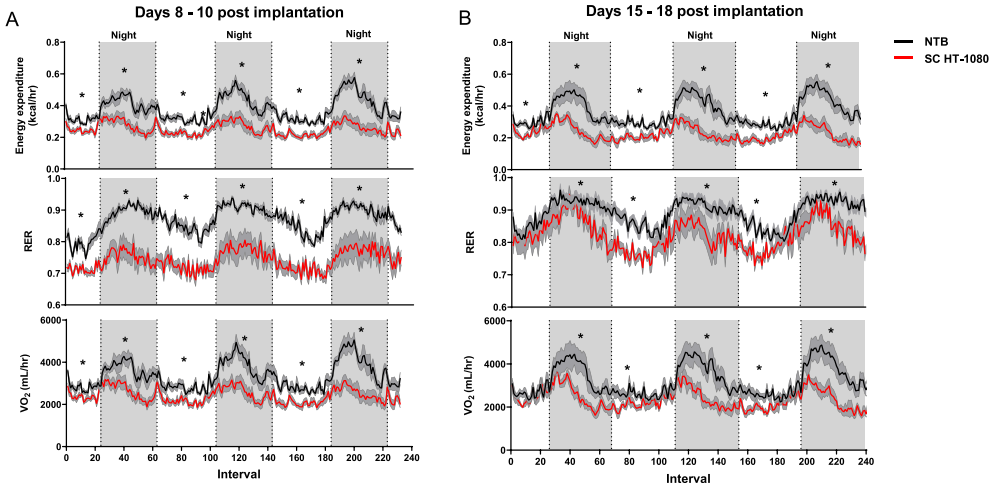

Figure 3 Whole-body metabolic changes in cancer cachexia. *(A and B)* The daytime and night-time energy expenditure, respiratory exchange ratio, and oxygen consumption (VO_2) (non-normalized) in tumour-bearing mice during early (Days 8–10) and late (Days 15–18) was lower than in the non-tumour-bearing (NTB) group. Shadows represented SEM. n = 8 animals/group; $^*P < 0.001$ by mixed-effects models. Data represented as mean ± SEM. RER = respiratory exchange ratio, SC = subcutaneous.

Several key circulating inflammatory biomarkers are elevated; derived from both the tumour and host

The HT-1080 tumour model is a human xenograft model, which allows for clear assessment of circulating inflammatory biomarkers produced by the tumour (human) and also the host (mouse). In the subcutaneous tumour model, several human biomarkers were elevated, including GDF-15, GDF-11, Activin A, IL-1β, IL-2, IL-4, IL-6, IL-8, tumor necrosis factor alpha (TNFα), and interferon gamma (IFNγ) (*Figure* 4). Consistent with muscle depletion, GDF-8 was decreased in tumour-bearing mice compared with NTB (*Figure* 4C). Interestingly, several biomarkers were also increased by the host (mouse): TNF alpha, IFNγ, KC/GRO, and IL-6 (*Figure* S3B, C, D, and I); IL-5 was reduced (*Figure* S3H). Host GDF-15 was unchanged (*Figure* S3A).

The HT-1080 tumour model results in skeletal and cardiac muscle wasting

Two key subsets of muscle tissue, skeletal and cardiac, were examined at the end of the study at both standard and thermoneutral housing temperature. Under both conditions, HT-1080 tumour-bearing mice demonstrated muscle loss in the fast-twitch fibre dominant muscles: gastrocnemius and tibialis anterior (*Table* 1). Similarly, heart weight was decreased, indicating the presence of cardiac atrophy (*Table* 1).

In the gastrocnemius and tibialis anterior skeletal muscles, expression of genes related to E3 ubiquitin ligase induction (*MuRF1*, *Atrogin-1*, *Foxo1*) and autophagy (*Bnip3*) in HT-1080 tumour-bearing mice compared with NTB tended to increase, but most did not reach statistical significance despite the large sample size (*Table* 2). In the soleus muscle, all of these genes were significantly increased approximately two-fold (*Table* 2). Cardiac atrophy was consistent with increased *Bnip3* expression (approximately two-fold) in tumour-bearing mice but with minimal induction of *MuRF1*, *Atrogin-1*, and *Foxo1* (*Table* 2).

We next evaluated the tibialis anterior muscle histologically including a comparison of the cross-sectional area (CSA) of muscle fibers between NTB and HT-1080 tumour-bearing mice (*Figure* 5A, B). TA muscle myofibers were smaller in the tumour-bearing mice compared with the NTB group (*Figure* 5A). The muscle fiber CSA distribution suggests that the overall fiber sizes were smaller in the HT-1080 tumour group (*Figure* 5B).

Skeletal muscle function (force) is dramatically reduced

Skeletal muscle force, maximum rate of contraction, and fatigability of HT-1080 tumour-bearing mice were assessed *in vivo* via the gastrocnemius/soleus complex (*Figure* 5C, D, S4A). Maximum twitch force was reduced by 15%, and maximum isometric force was reduced by >30% at maximal frequency (125 and 150 Hz) in tumour-bearing mice. Maximum rate of contraction was also reduced by >30% in the tumour-bearing group compared with the NTB controls (*Figure* 5D). However, HT-1080 tumour-bearing mice were unaffected when fatigability was assessed *in vivo* (*Figure* S4A).

Additionally, isolated muscle function of the tibialis anterior was assessed *in situ*. Maximum twitch and maximum isometric force were reduced by 18% in the tumour-bearing mice compared with NTB, but this did not achieve statistical significance (*Figure* S4B).

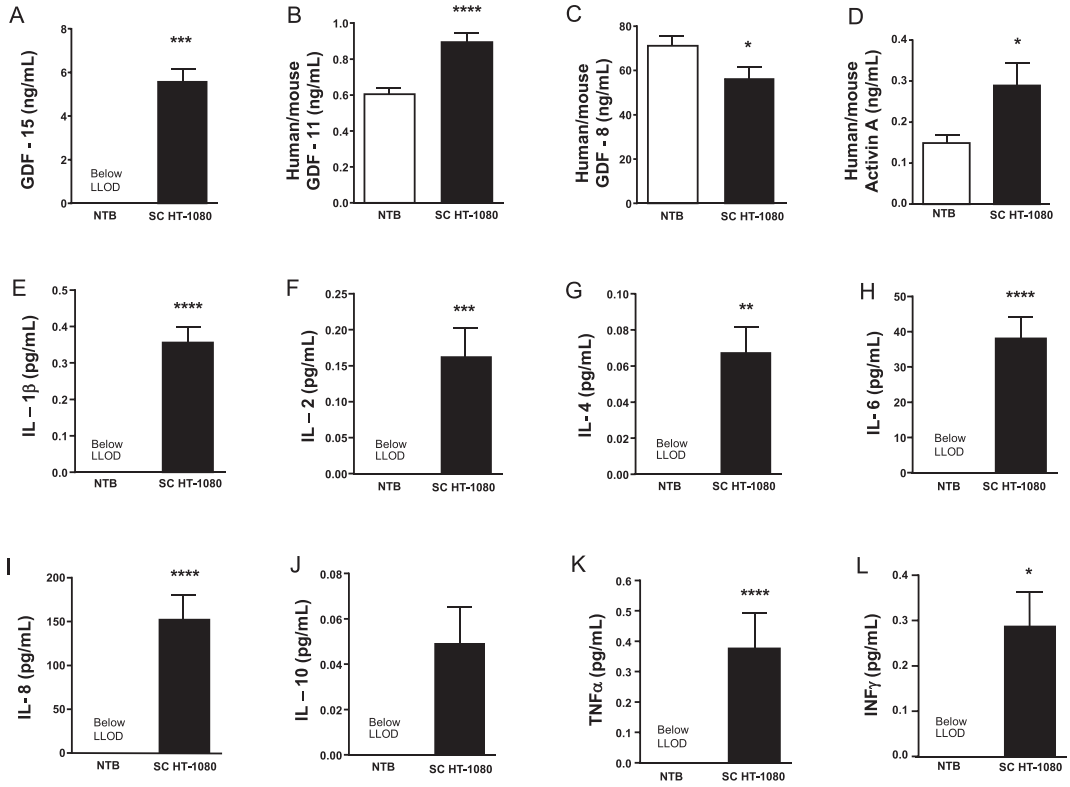

Figure 4 Several key circulating catabolic and pro-inflammatory cytokines are produced by the HT-1080 tumour (subcutaneous, thermoneutral). Catabolic factors: *(A)* growth differentiation factor 15 (GDF-15), *(B)* GDF-11, *(C)* GDF-8, and *(D)* Activin A. Pro-inflammatory cytokines: *(E)* interleukin (IL)-1β, *(F)* IL-2, *(G)* IL-4, *(H)* IL-6, *(I)* IL-8, *(J)* IL-10, *(K)* tumor necrosis factor alpha (TNFα), and *(L)interferon gamma* (INFγ). *n* = 15 animals/group; $*P < 0.05$; $**P < 0.01$; $***P < 0.001$; $****P < 0.0001$ by false discovery rate (FDR)-adjusted Student's *t*-test. These data represented as mean ± SEM. LLOD = lower limit of detection, NTB = non-tumor-bearing, SC = subcutaneous.

Table 1 Wet tissue weights of skeletal muscle and heart in subcutaneous HT-1080-induced cachexia

		Mean of wet tissue weights (mg)			
		Soleus muscle	Tibialis anterior muscle	Gastrocnemius muscle	Heart
Standard temperature (72°F ± 1°F)	NTB	6.7 ± 1.2	44.2 ± 3.3	120.1 ± 8.0	109.5 ± 10.7
	HT-1080	5.9 ± 1.2	30.2 ± 6.6	77.8 ± 6.0	85.1 ± 4.2
	P value	0.1578	0.0000	0.0001	0.0001
Thermoneutral (81°F ± 1°F)	NTB	7.9 ± 1.2	48.3 ± 4.4	137.4 ± 9.2	108.6 ± 7.3
	HT-1080	5.8 ± 1.4	35.0 ± 4.7	96.4 ± 18.4	88.7 ± 9.9
	P value	0.0025	0.0001	0.0001	0.0001

Robust decline in voluntary activity but not grip strength

Grip strength was measured as a potential surrogate for muscle strength. Although dramatic reductions in muscle mass and maximum force were observed in HT-1080 tumour-bearing mice, grip strength was only marginally reduced in the tumour-bearing mice (*Figure* 6A).

Ambulatory activity was also measured via infrared beam break technology in the CLAMS system. Tumour-bearing mice had reduced ambulatory activity during the dark cycle (the natural active cycle) as compared with NTB mice throughout the course of disease progression (*Figure* 6B). Mice have an intrinsic motivation to participate in wheel running activity, and therefore, we measured home cage voluntary wheel running distance in NTB and HT-1080 tumour-bearing mice as a representation of performance. Total daily wheel distance travelled was dramatically reduced in HT-1080 mice compared with NTB between Days 17 and 28 (*Figure* 6C). The reduction in wheel running distance in HT-1080 tumour-bearing mice coincided with ~10% body weight loss (*Figure* 6D). As the voluntary running wheel system only captures activity during wheel running, we monitored the average total cage motion (including access to the running wheel) of NTB and HT-1080 mice using

Table 2 mRNA expression level of atrophy genes in skeletal muscles and heart at thermoneutrality

Tissue type	Gene name	mRNA expression (fold changes) NTB	HT-1080	*P* value
Gastrocnemius	MuRF1	1.0 ± 0.4	2.5 ± 1.6	0.1021
	Atrogin-1	1.0 ± 0.4	2.1 ± 1.6	0.0639
	FOXO1	1.0 ± 0.5	1.5 ± 0.8	0.0001
	Bnip3	1.0 ± 0.5	1.3 ± 0.7	0.0696
Tibialis anterior	MuRF1	1.0 ± 0.2	3.7 ± 2.7	0.0595
	Atrogin-1	1.0 ± 0.2	3.1 ± 2.1	0.2831
	FOXO1	1.0 ± 0.3	3.3 ± 1.9	0.2124
	Bnip3	1.0 ± 0.2	2.7 ± 1.5	0.3132
Soleus	MuRF1	1.0 ± 0.4	2.2 ± 1.5	0.0017
	Atrogin-1	1.0 ± 0.6	2.4 ± 2.2	0.0052
	FOXO1	1.0 ± 0.4	3.9 ± 1.7	0.0002
	Bnip3	1.0 ± 0.4	2.2 ± 2.4	0.0002
Heart	MuRF1	1.0 ± 0.3	1.2 ± 0.2	0.1006
	Atrogin-1	1.0 ± 0.3	1.2 ± 0.3	0.1510
	FOXO1	1.0 ± 0.2	1.3 ± 0.3	0.0118
	Bnip3	1.0 ± 0.2	2.5 ± 0.8	0.0001

NTB = Non-Tumor Bearing mice; HT-1080 = Subcutaneous HT-1080 tumor-bearing mice.
Values are reported as mean ± standard deviation. n = 9-10 animals/group. MANOVA is applied for statistical test.

the VIUM system. Total average motion was much greater in the dark cycle than in the light cycle, and motion during the dark cycle was reduced in the HT-1080 mice compared with NTB mice from Day 11 to 18 (*Figure* 6E). This coincided with ~10% body weight loss (*Figure* 6F).

Anamorelin prevents but does not reverse cachexia in the HT-1080 tumour model

The effect of anamorelin on cachexia was examined in the HT-1080 tumour model in both prevention and intervention mode. In the prevention study, anamorelin treatment was initiated prior to weight loss on Day 8 post-tumour implantation. By Days 11–18, NTB mice that received anamorelin treatment had increased body weight in comparison with the NTB vehicle group (*Figure* 7A). Similarly, anamorelin administration in tumour-bearing mice increased body weight

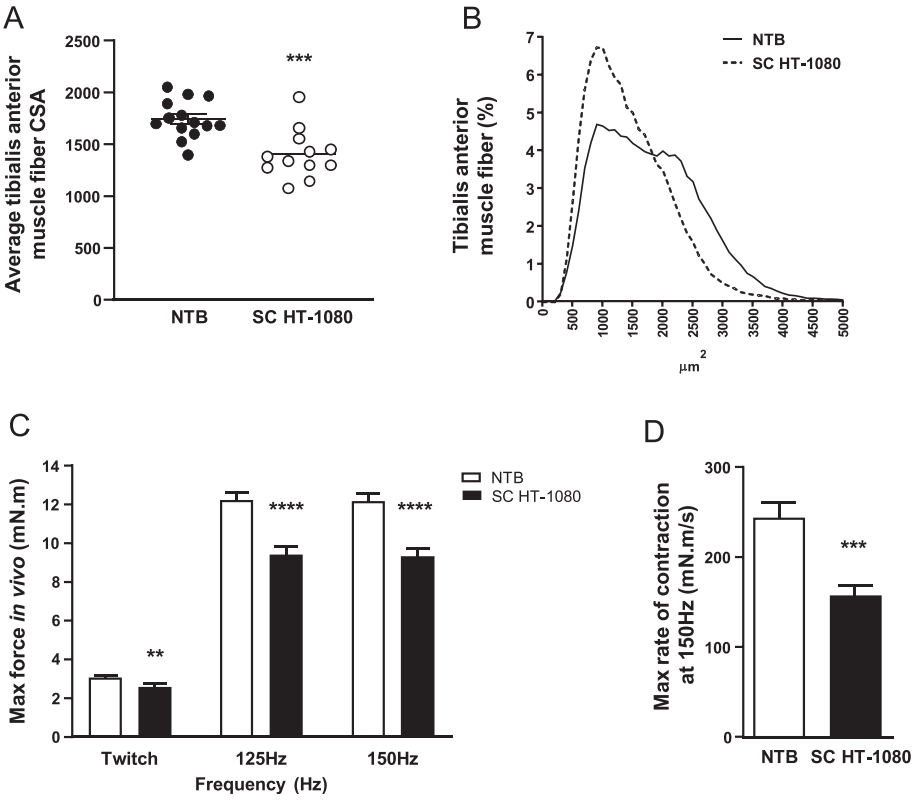

Figure 5 The HT-1080 tumour model (subcutaneous, thermoneutral) causes skeletal muscle wasting and reduced muscle function (force and fatigue). *(A and B)* Tibialis anterior (TA) fibre cross-sectional area reduced in HT-1080 tumour-bearing mice. TA muscle fiber average cross-sectional area distribution demonstrates that the overall fibre sizes are smaller in the HT-1080 tumour group. *n* = 11–14 animals/group. *(C)* Isometric twitch and maximum contraction of the gastrocnemius/soleus complex *in vivo* was reduced HT-1080 tumour-bearing mice. *n* = 13–14 animals/group. *(D)* Maximum rate of contraction of the gastrocnemius/soleus complex at 150 Hz during isometric contraction *in vivo* was decreased in HT-1080 tumour-bearing mice. *n* = 13–14 animals/group. $^{**}P < 0.01$; $^{***}P < 0.001$; $^{****}P < 0.0001$ by Student *t*-test, Kolmogorov–Smirnov test, and mixed-effects model. Data represented as mean ± SEM. CSA = cross-sectional area, NTB = non-tumor-bearing, SC = subcutaneous.

DOI: 10.1002/jcsm.12618

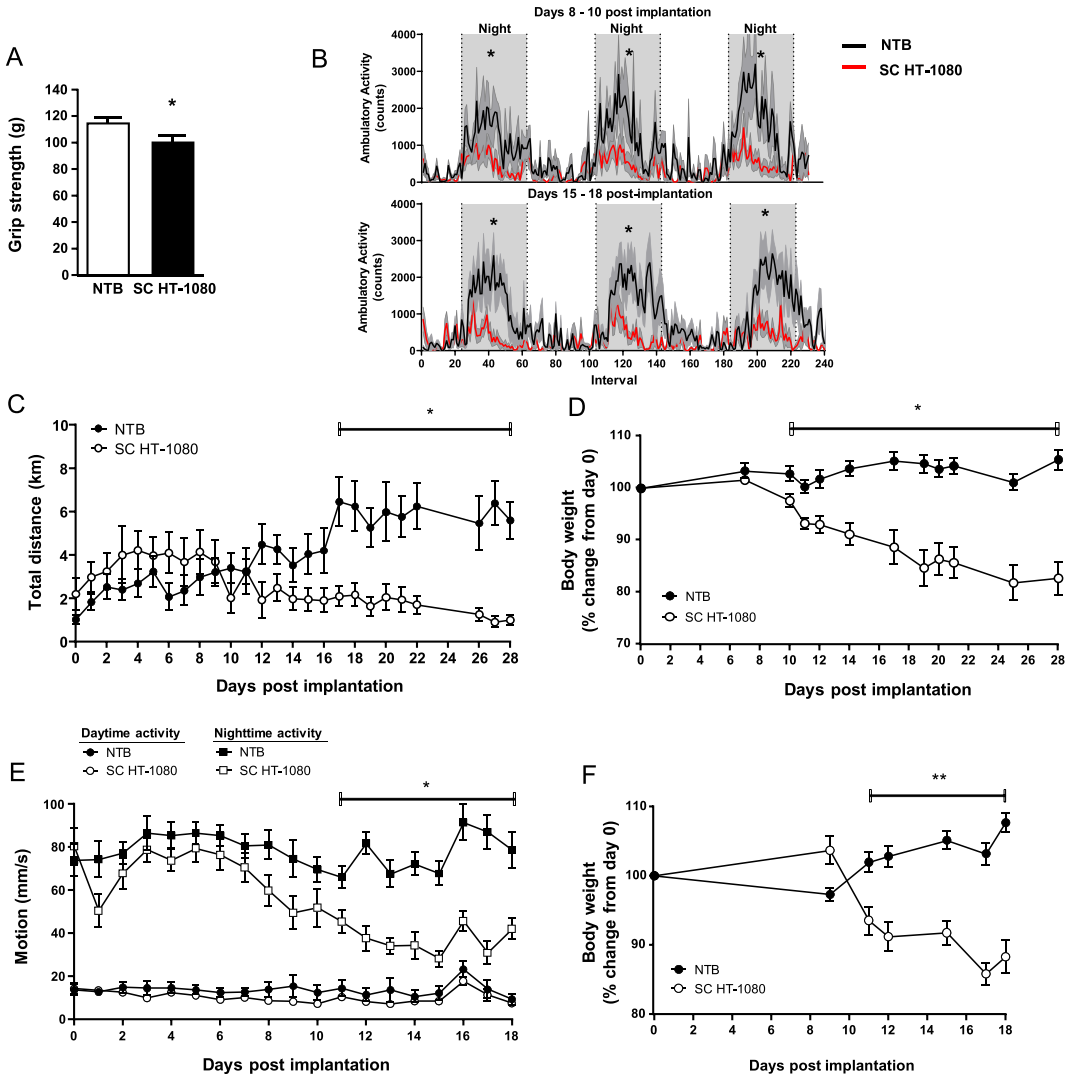

Figure 6 Robust decline in voluntary activity but not grip strength in HT-1080 tumour-bearing mice. *(A)* Muscle strength was assessed via grip strength measurement. Grip strength was reduced in HT-1080 tumour-bearing mice. n = 16 animals/group. *(B)* Ambulatory activity during early (Days 8–10) and late (Days 15–18) by comprehensive laboratory animal monitoring system home cage (CLAMS) system. The night-time ambulatory activity in SC HT-1080 tumour-bearing was lower than in non-tumour-bearing (NTB) control group. n = 8 animals/group; *$P < 0.05$ by mixed-effects models. *(C–F)* Total daily wheel running distance (Columbus magnetic wheels) was decreased in HT-1080 tumour-bearing mice from Day 17 to Day 28. Total daily spontaneous home cage motion (mm/s) measured in the VIUM Smart Cage system was decreased in HT-1080 tumour-bearing mice. n = 10–15 animals/group; *$P < 0.05$; **$P < 0.01$; grip strength were tested by Student's t-test. Pairwise comparison with false discovery rate (FDR) adjustment was applied for wheel running activation and motion, and comparison of body weight changes with mixed-effects models. Data represented as mean ± SEM. NTB = non-tumor-bearing, SC = subcutaneous.

from Day 11 post-implantation compared with the vehicle-treated tumour control group (*Figure* 7A). Anamorelin increased fat mass (*Figure* 7B) but not lean mass (*Figure* 7C, *Table* 3). However, lean mass assessed by echo magnetic resonance imaging (*Figure* 7C) was not significantly reduced in the HT-1080 vehicle group compared with NTB vehicle likely owing to the study duration (study stopped at 10% weight loss). Skeletal muscle tissue weight, which is a more sensitive endpoint, was decreased in the gastrocnemius and tibialis anterior but not quadriceps in the HT-1080 vehicle group compared with NTB vehicle (*Table* 3). Food intake was decreased in tumour-bearing mice compared with NTB, and as expected, anamorelin increased food intake in NTB mice (*Figure* 7D). Consistent with the body weight effect, anamorelin normalized food intake in tumour-bearing mice (*Figure* 7D). Tumour growth was unaffected by the treatment (*Figure* 7E). In the intervention study, anamorelin treatment was initiated on Day 13 post-tumour implantation when ~10% weight loss was achieved. Unlike in the prevention study, anamorelin did not increase body weight in tumour-bearing mice (*Figure* 7F). There was a small reduction in tumour weight with anamorelin treatment (*Figure* 7G).

DOI: 10.1002/jcsm.12618

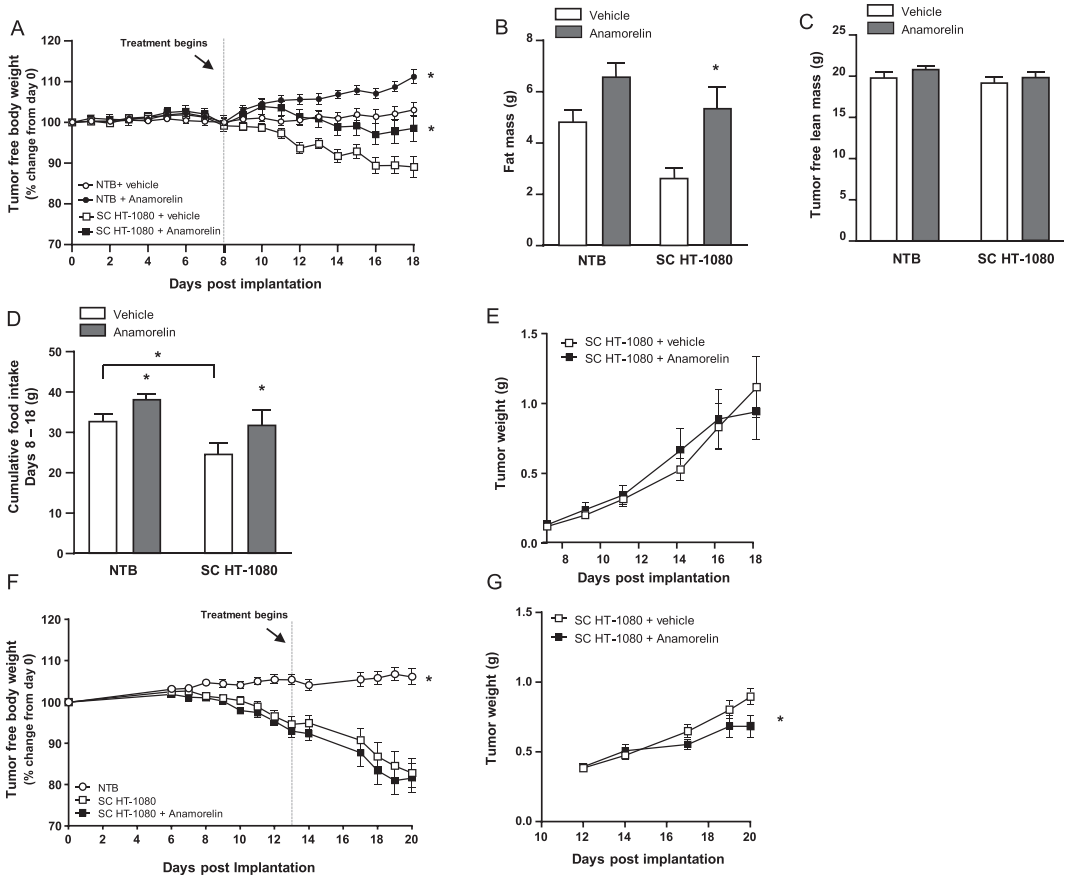

Figure 7 Anamorelin prevents but does not reverse cachexia in the HT-1080 tumour model (subcutaneous, thermoneutral). *(A–F)* Anamorelin treatment was initiated on Day 8 post-implantation prior to weight loss (prevention). In both non-tumour-bearing (NTB) and HT-1080 tumour-bearing mice, anamorelin increased *(A)* tumour-free body weight and *(B)* fat mass but not *(C)* tumour-free lean mass. *(D)* Anamorelin also increased cumulative food intake in both NTB and HT-1080 tumour-bearing mice (Days 8–18). *(E)* Tumour weight was not affected by anamorelin treatment. n = 7–11 animals/group. *(F and G)* Anamorelin treatment was initiated on Day 13 post-implantation at ~10% weight loss (intervention). In HT-1080 tumour-bearing mice, *(F)* anamorelin did not increase tumour-free body weight. *(G)* Tumour weight was decreased by anamorelin treatment at the end of the study. n = 10 animals/group, $^*P < 0.05$; comparison of body weight changes with mixed-effects models. Comparison of body composition (fat and lean mass) and food intake changes with one-way analysis of variance. Comparison of tumour weight by mixed-effect models. Data represented as mean ± SEM. SC = subcutaneous.

Discussion

Cancer cachexia is a complex metabolic disease with unmet medical need. Although numerous rodent models have been described, none are identical to the human disease. Therefore, the development of new preclinical models that simulate some of the physiological, biochemical, and clinical characteristics of the human disease is needed. The HT-1080 human fibrosarcoma cell line is most commonly used to study the effects of anti-cancer mechanisms and possesses an activating *RAS* mutation like many tumour models.[19–21] Although sarcomas are generally not recognized as the most highly cachectic tumours,[2] HT-1080 tumours secrete several relevant pro-cachectic factors such as GDF-15, Activin A, and IL-6; and weight loss has been reported in this tumour model.[22] This raised the possibility that this model could provide a valuable opportunity to understand cachexia mechanisms and assess efficacy of new therapeutic agents preclinically. Therefore, we set out to determine whether the HT-1080 tumour model recapitulates the characteristics of human cachexia. As part of the model validation effort, we also tested the efficacy of ghrelin receptor activation using the small molecule anamorelin, because it is one of few mechanisms supported by clinical data in cachexia. Additionally, we determined optimal model conditions and examined technical performance.

In our investigation, we have confirmed several advantages of the subcutaneous HT-1080 tumour model over existing tumour cell models. This model is commercially available and reproducible in that the cachexia phenotype is consistently observed across experiments (and cell line lots, cell

Table 3 Wet tissue weights of each skeletal muscle in subcutaneous HT-1080 following anamorelin treatment.

Skeletal muscle type	Group	Mean of wet tissue weights (mg)
Tibialis anterior	NTB + vehicle	40.1 ± 7.2
	NTB + anamorelin	37.1 ± 5.4
	HT-1080 + vehicle	32.7 ± 3.9*
	HT-1080 + anamorelin	33.1 ± 6.8†
Gastrocnemius	NTB + vehicle	126.1 ± 16.4
	NTB + anamorelin	131.2 ± 11.8
	HT-1080 + vehicle	108.9 ± 14.9*
	HT-1080 + anamorelin	114.6 ± 16.8
Quadriceps	NTB + vehicle	167.9 ± 19.8
	NTB + anamorelin	167.0 ± 17.4
	HT-1080 + vehicle	151.6 ± 25.1
	HT-1080 + anamorelin	145.7 ± 24.72

Values are reported as mean ± standard deviation; n = 9-11 animals/group. Multivariate analysis of variance is applied for statistical test.
HT-1080, subcutaneous HT-1080 tumour-bearing mice; NTB, non-tumour-bearing mice.
*$P < 0.05$ NTB + vehicle vs. HT-1080 + vehicle.
†#$P < 0.05$ NTB + vehicle vs. HT-1080 + anamorelin.

passages, and physical location of experiments conducted); however there is some modest variability in the timing of cachexia development. In most (six out of seven) of our experiments (summarized in *Table* S2), despite some differences in experimental conditions like access to wheel running, 10% weight loss was consistently achieved at 12–14 days post-implantation. In one experiment, 10% weight loss was reached 25% faster at 9 days post-implantation. Given that some heterogeneity is present, we propose this risk can be mitigated by using predefined body weight loss goals to trigger intervention start. In addition, cachexia was observed with both tumour cell inoculation sites, and there was no evidence of kidney dysfunction even with heterotopic implantation, which makes for easier interpretation of cachexia interventions.

Depending on experimental design (i.e. sample size and timing of intervention initiation), there is opportunity for ~2 weeks of treatment in the HT-1080 model. In Lerner *et al*. 2016[22], this treatment window was sufficient to demonstrate efficacy of an appetite stimulant and muscle anabolic mechanism; however, this is also likely influenced by the robustness of the mechanism being evaluated. Currently available tumour models do not offer a notably longer therapeutic window; however, the onset of cachexia is generally less rapid in the genetic models. Interestingly, the timing of disease progression in mice compared with humans is not so profoundly different if compared in the context of lifespan differences across species. For example, if the limited adulthood lifespan (defined as reproductive viability in females) of a mouse compared with a human is taken into consideration, there is a 17-fold difference. Therefore, a cachexia definition of >10% body weight loss in 6 months in patients is the equivalent of ~10 days in a mouse and within the range of this model.

From a physiological perspective, the phenotype of this model is consistent with the features of cachexia described in patients.[1,2] This includes elevation of several catabolic and pro-inflammatory cytokines, anorexia, weight loss, fat and lean mass loss, reduced muscle strength, and activity. The body weight loss and body composition changes in the HT-1080 model are comparable with other more severe cachectic tumour models in the literature such as C26 where a drop in body weight of over 20% and muscle atrophy of over 30% is common,[28,29] although we acknowledge that the severity of the cachectic phenotype in the C26 model is dependent on the subclone being used. Similarly, the more recently described genetic models KPC and KPP also display large degrees of adipose tissue loss and muscle wasting with steep survival curves; however, in the case of KPC, the phenotype is dependent on the tumour cell route of administration.[5,7,8] In general, the LLC tumour model shows a less severe phenotype with no changes in adipose tissue and only 3.4% reduction in lean mass,[30] and again this is subclone dependent.

Skeletal muscle wasting, a hallmark of cachexia, is a key feature of this model demonstrated by decreased lean mass, muscle weight, and muscle fiber CSA. Interestingly, the elevation of genes related to the ubiquitin pathway and autophagy in the HT-1080 model was modest and did not reach statistical significance in both the gastrocnemius and tibialis anterior muscles. This profile is unlike the typical large increase reported in the C26 and LLC tumour models and is more similar to that reported in the KPP mouse tumour model and cachectic pancreatic cancer patients.[7] This suggests that the HT-1080 model has greater similarity to human cachexia than other common tumour models, and a future comparative study of the muscle transcriptome profile of the HT-1080 model is warranted.

Evaluation of body composition in the HT-1080 model highlights that adipose tissue may be more sensitive than skeletal muscle to cancer cachexia-induced catabolism. Reports from both clinical trials and longitudinal observation studies in cachexia patients suggest that the loss of both adipose and muscle mass has been reported to varying degrees and can be influenced by stage of disease and cancer type. For example, the anamorelin Phase 3 placebo-controlled trials[31] enrolled patients with unresectable stage III or IV non-small-cell lung cancer and cachexia (defined as involuntary weight loss of ≥5% within the previous 6 months, or body mass index < 20 kg/m^2). Body composition was measured using dual-energy X-ray absorptiometry. In ROMANA 1, it was reported that over 12 weeks, the placebo group had similar reductions in adipose and lean body mass (LBM) (adipose, 0.6%; LBM, 0.5%), whereas in ROMANA 2, there was greater LBM loss than adipose mass (adipose, 0.2%; LBM, 1.1%).

Furthermore, in a longitudinal observation study,[32] it was reported that loss of adipose and muscle tissue was measured using computed tomography imaging in a population cohort of 368 advanced cancer patients including lung, colorectal, and pancreatic cancer and cholangiocarcinoma, with tumour types associated with highest prevalence of cachexia.[2] On average, the population showed a simultaneous loss of muscle and adipose tissue and were progressively more catabolic over time proceeding death. There was a positive correlation between the amount of muscle loss and fat loss with the median adipose tissue loss greater than the median skeletal muscle loss across all the tumour types examined.[32] The fat and muscle mass loss in the HT-1080 tumour model is consistent with reports from cancer cachexia patients.

A key point of discussion in the cachexia field is whether therapies that increase skeletal muscle mass also result in healthy functional muscle. Histological CSA quantification of the tibialis anterior muscle revealed substantial atrophy of the myofibers in HT-1080 tumour-bearing mice. Currently, it is not clear whether cancer cachexia preferentially acts on glycolytic fibres (IIb/x) or oxidative slow-twitch fibres.[33,34] In our studies, we directly measured skeletal muscle function (force and fatigue) in a setting that is independent of behaviour. Perhaps unsurprisingly, when fatigue was assessed *in vivo*, no difference in fatigue-related endpoints was observed. This is likely due to the aforementioned preservation of oxidative capacity and oxidative fibres (I/IIa) in cancer cachexia.[33]

Rodent tumour models can also be leveraged to compare a variety of endpoints related to physical function and activity including grip strength, locomotion, and voluntary exercise. The grip strength revealed a significant decrease in tumour-bearing mice, although the decrease was subtle relative to the magnitude of the overall loss in muscle mass and CSA. Conversely, when muscle function was examined via maximum force generation *in vivo*, maximum twitch force, maximum isometric tetanic force, and maximum rate of contraction were greatly reduced in HT-1080 tumour-bearing animals. Our hypothesis for this discrepancy in 'muscle function' assays is two-fold: (i) the sensitivity of grip strength measurements is habitually poor, and (ii) grip strength inherently introduces high levels of human technical variability and mouse behavioural variability. This brings into question whether grip strength is a reliable method to assess muscle quality and strength given its high variability and relevance as an assessment of strength vs. motivation. Furthermore, we confirm that when muscle function is measured directly, the severity in functional decline is in line with the severity of CSA and muscle atrophy. These findings are also supported by previous reports from other cancer cachectic models demonstrating impaired maximum force generation with no decline in fatigue.[11]

Currently, there is much emphasis on quality of life-related endpoints in cachexia patients, highlighting outcomes such as appetite, fatigue, and activity. In patients, appetite/food intake measurement is limited to questionnaires, but in mice, it can be directly quantitated with careful assessment. Along with appetite, fatigue (physical and psychological) is one of the most notable manifestations of cachexia, and therefore, it is important that cachexia models recapitulate this endpoint. Fatigue is often described in terms of the impact on daily life and activities when patients are no longer able to participate in their favourite activities. Advances in biosensor technology may enable more quantitative assessments of activity in patients, and several groups are working to validate these devices in patients. We chose to examine activity in our mouse model by monitoring voluntary wheel locomotion and overall cage activity. Wheel running is viewed as a voluntary (allows for self-motivation) pleasurable activity for mice[35,36] and can be administered with unlimited access and without aversive stimuli. We found that overall cage activity and wheel use were reduced during disease progression in the HT-1080 tumour-bearing mice. This change is consistent with our data showing reduced energy availability, skeletal muscle function, and metabolic capacity. It is also possible that tumour mass (between 5% and 10% of body weight) and/or any associated pain or discomfort may contribute to reduced activity. Furthermore, a comparison of experiments including wheel running vs. those without wheel running does not reveal an obvious protective effect of exercise on weight loss. However, ideally, a single study including both wheel and non-wheel running groups and examination of body weight and skeletal muscle mass/function would be needed to conclusively address this question. Future studies could target these components to better understand the relevance of each as key contributors.

Chronic inflammation and elevated cytokine levels have been implicated as drivers of cancer cachexia.[37–40] The HT-1080 tumour model is very interesting from a therapeutic perspective because it is characterized by the elevation of multiple circulating factors implicated in cachexia (i.e. GDF-15, IL-6, and Activin A). It was reported that an anti-GDF-15 antibody was sufficient to reverse weight loss and anorexia in this model.[22] For model validation, we thought it was valuable to evaluate the efficacy of one of the few anti-cachexia agents supported by clinical efficacy data, anamorelin (ghrelin analogue). Although anamorelin is not currently an approved therapy, it has been reported to increase skeletal muscle mass and improve appetite in non-small-cell lung carcinoma patients with cachexia[31]. Although the characteristics of this model do not allow us to directly match the disease stage when treatment was initiated in the clinical setting, we found that early treatment with anamorelin was important to increase food intake and body weight in this cancer cachexia mouse model. As ghrelin appetite and body weight regulation are mediated in part by the melanocortin pathway,[41] and it has been reported that neuroinflammation in cachexia suppresses the melanocortin system,[42] the lack of efficacy is likely attributed to greater cytokine production as the tumour progresses and the subsequent neuroinflammation. Different

from clinical reports,[31] we found that anamorelin increased fat mass but not LBM. This may be explained by the young age of the mice or shorter duration of treatment compared with those of patients, although this will require further consideration.

Although the HT-1080 tumour model reflects many of the physiological, biochemical, and clinical characteristics of human cachexia, this model is not without limitations. Fibrosarcoma is a rare tumour type that is not typically associated with cachexia.[2] We report that multiple cytokines are elevated in this model; however, the mice are immunocompromised, which does not reflect the immune profile of human cachexia. Tumour development is rapid in this model and does not recapitulate the tumour microenvironment of human cancer. Furthermore, HT-1080 cells are not sensitive to chemotherapy, and therefore, chemotherapy combination studies cannot be performed nor can longer-term testing of cachexia interventions because tumour progression ultimately limits study length.

Given the heterogeneity of cancer cells and cachexia, it is likely most prudent to evaluate/validate mechanisms across multiple models rather than try to develop a single gold standard model. Therefore, despite the limitations of the HT-1080 tumour model we have described, we think this model is an improvement over existing models that utilize tumour cell lines and will add to the list of model options for the cachexia researcher to improve our understanding of key mechanisms responsible for anorexia and tissue wasting. Furthermore, it is essential to understand the characteristics of each model in detail, because cachexia is multifactorial and researchers should choose a model appropriate for the hypothesis. In summary, we demonstrate that the subcutaneous HT-1080 tumour model is reproducible and displays key features of clinical cachexia, such as perturbations of energy balance, impairment of muscle function and performance, and elevation of circulating cytokines and pro-cachectic factors. Consistent with clinical reports, anamorelin treatment in this model was most beneficial when administered earlier in disease progression. The HT-1080 tumour model is therefore a valuable preclinical model for cancer cachexia research and drug discovery.

Acknowledgements

We would like to thank Darla Dash for *in vivo* support, Gary Seitis and Andrew Robertson for histology support, and Alan Opsahl for image analysis support. The authors of this manuscript certify that they comply with the ethical guidelines for authorship and publishing in the *Journal of Cachexia, Sarcopenia and Muscle*.[43]

Online supplementary material

Additional supporting information may be found online in the Supporting Information section at the end of the article.

Figure S1 (A) Heterotopic HT-1080 or (B) subcutaneous HT-1080 body weight changes post-implantation at standard housing conditions. (C) Heterotopic HT-1080 tumor and primary kidney tissue weight was measured on day 8 (n = 3) and day 15 (n = 15) post-implantation. (D) Histological examination of tumors from heterotopic (left image) and subcutaneous (center image) models housed at standard temperature, and from the subcutaneous model housed at thermoneutral temperature (right image). Sections were stained with hematoxylin and eosin. Scale bar: 300 uM. (E and F) Kidney function in heterotopic HT-1080 tumor-bearing mice in standard housing conditions assessed via (E) blood urine nitrogen (BUN) and (F) serum creatine measured at the end of the study on day 15. n = 11–15 animals/group; $^{*}P < 0.05$; $^{**}P < 0.01$; Comparison of tumor weight, serum BUN, and creatine level with Student's t-test. Comparison of body weight changes with mixed effects models. Data represented as mean ± SEM.

Figure S2 (A-C) Subcutaneous HT-1080 model at thermoneutral housing temperature during CLAMS energy expenditure assessment. (A) Tumor free body weight changes post-implantation expressed in grams, (B) Tumor free body weight changes post-implantation expressed in percent (C) tumor growth, and (D) cumulative food intake days 14-15, (E) Daytime and nighttime energy expenditure normalized by tumor free body weight. n = 7–8 animals/group; $^{*}P < 0.05$; $^{**}P < 0.01$; $^{****}P < 0.0001$; Comparison of body weight changes and energy expenditure by mixed effects models. Comparison of food intake changes with Student's t-test. Data represented as mean ± SEM.

Figure S3 Mouse plasma protein profile of catabolic and pro-inflammatory cytokines in the subcutaneous HT-1080 tumor model at thermoneutral housing temperature. n = 15–16 animals/model; $^{*}P < 0.05$; $^{**}P < 0.01$; $^{****}P < 0.0001$ by FDR adjusted Student's t-test. These data represented as mean ± SEM.

Figure S4 (A) Isometric contraction fatigue profile of the gastrocnemius/soleus complex *in vivo* of NTB and HT-1080 tumor-bearing mice (subcutaneous, thermoneutral). n = 13–14 animals/group. (B) Isometric twitch and maximal tension of *in situ* stimulated TA muscle was reduced in HT-1080 tumor-bearing mice. n = 11–13 animals/group. Mixed effects and Student's t-test. Data are expressed as mean ± SEM.

Conflict of interest

B.B., S.J., J.G., M.B., C.H., B.L., S.Q., Z.W., R.M.E., M.P., H.K., and D.M.B. are employees of Pfizer Inc. All experiments were funded by Pfizer Inc.

References

1. Fearon K, Strasser F, Anker SD, Bosaeus I, Bruera E, Fainsinger RL, et al. Definition and classification of cancer cachexia: an international consensus. *Lancet Oncol* 2011;**12**:489–495.
2. Baracos VE, Martin L, Korc M, Guttridge DC, Fearon KCH. Cancer-associated cachexia. *Nat Rev Dis Primers* 2018;**4**:17105.
3. Bennani-Baiti N, Walsh D. Animal models of the cancer anorexia-cachexia syndrome. *Support Care Cancer* 2011;**19**:1451–1463.
4. Ishida J, Saitoh M, Springer J. Single-nucleotide polymorphisms in cachexia-related genes: can they optimize the treatment of cancer cachexia? *J Cachexia Sarcopenia Muscle* 2017;**8**:516–517.
5. Michaelis KA, Zhu X, Burfeind KG, Krasnow SM, Levasseur PR, Morgan TK, et al. Establishment and characterization of a novel murine model of pancreatic cancer cachexia. *J Cachexia Sarcopenia Muscle* 2017;**8**:824–838.
6. Penna F, Bonetto A, Aversa Z, Minero VG, Rossi Fanelli F, Costelli P, et al. Effect of the specific proteasome inhibitor bortezomib on cancer-related muscle wasting. *J Cachexia Sarcopenia Muscle* 2016;**7**:345–354.
7. Talbert EE, Cuitino MC, Ladner KJ, Rajasekerea PV, Siebert M, Shakya R, et al. Modeling human cancer-induced cachexia. *Cell Rep* 2019;**28**:1612–1622, e4.
8. Danai LV, Babic A, Rosenthal MH, Dennstedt EA, Muir A, Lien EC, et al. Altered exocrine function can drive adipose wasting in early pancreatic cancer. *Nature* 2018;**558**:600–604.
9. Matsumoto T, Iida M, Nakamura S, Hizawa K, Mizuno M, Yao T, et al. Depressed adenoma of the duodenum in patients with familial adenomatous polyposis: endoscopic and immunohistochemical features. *Cancer* 1999;**86**:1414–1420.
10. Murphy KT, Chee A, Trieu J, Naim T, Lynch GS. Importance of functional and metabolic impairments in the characterization of the C-26 murine model of cancer cachexia. *Dis Model Mech* 2012;**5**:533–545.
11. Norden DM, Bicer S, Clark Y, Jing R, Henry CJ, Wold LE, et al. Tumor growth increases neuroinflammation, fatigue and depressive-like behavior prior to alterations in muscle function. *Brain Behav Immun* 2015;**43**:76–85.
12. Tanaka Y, Eda H, Tanaka T, Udagawa T, Ishikawa T, Horii I, et al. Experimental cancer cachexia induced by transplantable colon 26 adenocarcinoma in mice. *Cancer Res* 1990;**50**:2290–2295.
13. Llovera M, Garcia-Martinez C, Lopez-Soriano J, Carbo N, Agell N, Lopez-Soriano FJ, et al. Role of TNF receptor 1 in protein turnover during cancer cachexia using gene knockout mice. *Mol Cell Endocrinol* 1998;**142**:183–189.
14. Goncalves MD, Hwang SK, Pauli C, Murphy CJ, Cheng Z, Hopkins BD, et al. Fenofibrate prevents skeletal muscle loss in mice with lung cancer. *Proc Natl Acad Sci U S A* 2018;**115**:E743–E752.
15. Lee JW, Komar CA, Bengsch F, Graham K, Beatty GL. Genetically engineered mouse models of pancreatic cancer: the KPC model (LSL-Kras(G12D/+);LSL-Trp53(R172H/+);Pdx-1-Cre), its variants, and their application in immuno-oncology drug discovery. *Curr Protoc Pharmacol* 2016;**73**:14–39.
16. Bonetto A, Aydogdu T, Kunzevitzky N, Guttridge DC, Khuri S, Koniaris LG, et al. STAT3 activation in skeletal muscle links muscle wasting and the acute phase response in cancer cachexia. *PLoS ONE* 2011;**6**:e22538.
17. Talbert EE, Metzger GA, He WA, Guttridge DC. Modeling human cancer cachexia in colon 26 tumor-bearing adult mice. *J Cachexia Sarcopenia Muscle* 2014;**5**:321–328.
18. Yanagihara K, Kubo T, Iino Y, Mihara K, Morimoto C, Seyama T, et al. Development and characterization of a cancer cachexia model employing a rare human duodenal neuroendocrine carcinoma-originating cell line. *Oncotarget* 2019;**10**:2435–2450.
19. Denais CM, Gilbert RM, Isermann P, McGregor AL, te Lindert M, Weigelin B, et al. Nuclear envelope rupture and repair during cancer cell migration. *Science* 2016;**352**:353–358.
20. Schreiber-Brynzak E, Klapproth E, Unger C, Lichtscheidl-Schultz I, Goschl S, Schweighofer S, et al. Three-dimensional and co-culture models for preclinical evaluation of metal-based anticancer drugs. *Invest New Drugs* 2015;**33**:835–847.
21. Zhang L, Hill RP. Hypoxia enhances metastatic efficiency in HT1080 fibrosarcoma cells by increasing cell survival in lungs, not cell adhesion and invasion. *Cancer Res* 2007;**67**:7789–7797.
22. Lerner L, Tao J, Liu Q, Nicoletti R, Feng B, Krieger B, et al. MAP 3K11/GDF15 axis is a critical driver of cancer cachexia. *J Cachexia Sarcopenia Muscle* 2016;**7**:467–482.
23. Palandra J, Quazi A, Fitz L, Rong H, Morris C, Neubert H. Quantitative measurements of GDF-8 using immunoaffinity LC-MS/MS. *Proteomics Clin Appl* 2016;**10**:597–604.
24. Northrup R, Kuroda K, Duus EM, Barnes SR, Cheatham L, Wiley T, et al. Effect of ghrelin and anamorelin (ONO-7643), a selective ghrelin receptor agonist, on tumor growth in a lung cancer mouse xenograft model. *Support Care Cancer* 2013;**21**:2409–2415.
25. Cameron KM, Speakman JR. The extent and function of 'food grinding' in the laboratory mouse (*Mus musculus*). *Lab Anim* 2010;**44**:298–304.
26. Chand HS, Du X, Ma D, Inzunza HD, Kamei S, Foster D, et al. The effect of human tissue factor pathway inhibitor-2 on the growth and metastasis of fibrosarcoma tumors in athymic mice. *Blood* 2004;**103**:1069–1077.
27. Steinstraesser L, Jacobsen F, Schubert C, Gevers K, Stricker I, Steinau HU, et al. Establishment of a primary human sarcoma model in athymic nude mice. *Hum Cell* 2010;**23**:50–57.
28. Sun R, Zhang S, Lu X, Hu W, Lou N, Zhao Y, et al. Comparative molecular analysis of early and late cancer cachexia-induced muscle wasting in mouse models. *Oncol Rep* 2016;**36**:3291–3302.
29. Liu D, Qiao X, Ge Z, Shang Y, Li Y, Wang W, et al. IMB0901 inhibits muscle atrophy induced by cancer cachexia through MSTN signaling pathway. *Skelet Muscle* 2019;**9**:8.
30. Nicholson JR, Kohler G, Schaerer F, Senn C, Weyermann P, Hofbauer KG. Peripheral administration of a melanocortin 4-receptor inverse agonist prevents loss of lean body mass in tumor-bearing mice. *J Pharmacol Exp Ther* 2006;**317**:771–777.
31. Temel JS, Abernethy AP, Currow DC, Friend J, Duus EM, Yan Y, et al. Anamorelin in patients with non-small-cell lung cancer and cachexia (ROMANA 1 and ROMANA 2): results from two randomised, double-blind, phase 3 trials. *Lancet Oncol* 2016;**17**:519–531.
32. Prado CM, Lieffers JR, Bowthorpe L, Baracos VE, Mourtzakis M, McCargar LJ. Sarcopenia and physical function in overweight patients with advanced cancer. *Can J Diet Pract Res* 2013;**74**:69–74.
33. Fearon KC, Glass DJ, Guttridge DC. Cancer cachexia: mediators, signaling, and metabolic pathways. *Cell Metab* 2012;**16**:153–166.
34. Johns N, Hatakeyama S, Stephens NA, Degen M, Degen S, Frieauff W, et al. Clinical classification of cancer cachexia: phenotypic correlates in human skeletal muscle. *PLoS ONE* 2014;**9**:e83618.
35. Izumo N, Ishibashi Y, Ohba M, Morikawa T, Manabe T. Decreased voluntary activity

and amygdala levels of serotonin and dopamine in ovariectomized rats. *Behav Brain Res* 2012;**227**:1–6.
36. Roberts MD, Gilpin L, Parker KE, Childs TE, Will MJ, Booth FW. Dopamine D1 receptor modulation in nucleus accumbens lowers voluntary wheel running in rats bred to run high distances. *Physiol Behav* 2012;**105**:661–668.
37. Evans WJ, Morley JE, Argiles J, Bales C, Baracos V, Guttridge D, et al. Cachexia: a new definition. *Clin Nutr* 2008;**27**:793–799.
38. Burfeind KG, Michaelis KA, Marks DL. The central role of hypothalamic inflammation in the acute illness response and cachexia. *Semin Cell Dev Biol* 2016;**54**:42–52.
39. Schiessel DL, Baracos VE. Barriers to cancer nutrition therapy: excess catabolism of muscle and adipose tissues induced by tumour products and chemotherapy. *Proc Nutr Soc* 2018;**77**:394–402.
40. Lerner L, Hayes TG, Tao N, Krieger B, Feng B, Wu Z, et al. Plasma growth differentiation factor 15 is associated with weight loss and mortality in cancer patients. *J Cachexia Sarcopenia Muscle* 2015;**6**:317–324.
41. Muller TD, Nogueiras R, Andermann ML, Andrews ZB, Anker SD, Argente J, et al. Ghrelin. *Mol Metab* 2015;**4**:437–460.
42. Dwarkasing JT, Marks DL, Witkamp RF, van Norren K. Hypothalamic inflammation and food intake regulation during chronic illness. *Peptides* 2016;**77**:60–66.
43. von Haehling S, Morley JE, Coats AJS, Anker SD. Ethical guidelines for publishing in the *Journal of Cachexia, Sarcopenia and Muscle*: update 2019. *J Cachexia Sarcopenia Muscle* 2019;**10**:1143–1145.